High Resolution Ultrasonic Imaging in Stiffened Composite Panels by Robust Data-Driven Matched Field Processing

CHENGYANG HUANG, ALI ZARE HOSSEINZADEH
and FRANCESCO LANZA DI SCALEA

ABSTRACT

Ultrasonic imaging techniques are commonly deployed using sparse transducer arrays operated under plane wave beamforming such as delay-and-sum or time migration methods. However, in complex aerospace structures such as stiffened composite panels, wave refraction and dispersion effects significantly complicate the beamforming process. To address these challenges, the complexity of the propagating waves for impact and damage imaging can be best leveraged by using data-driven Matched Field Processing (MFP) techniques. These methods are effectively used in underwater acoustics but much less employed in SHM/NDE. This work introduces both passive and active beamforming techniques within the data-driven MFP framework using a sparse array of ultrasonic piezoelectric transducers applied to a complex aerospace panel. In particular, the broadband Coherent White Noise Constraint (C-WNC) beamformer is applied to cross correlate data-driven models and the data of interest. The C-WNC algorithm is robust against model mismatch and achieves high resolution and contrast. Its efficacy is demonstrated through passive imaging of hammer impacts on a stiffened composite panel. For damage imaging, where the damage scatterings typically act as secondary sources, conventional adaptive beamformers primarily focus on the active sources, such as a transmitter element or hammer impacts. To increase the sensitivity to structural damage in the covariance matrix, the "active" inter-element transfer functions are reconstructed by estimating the normalized cross-power spectrum between two receiver elements. This reconstruction is achieved passively by observing the structural response to a series of hammer impacts. By averaging the covariance matrix using only few hammer impacts, the C-WNC algorithm is shown to successfully image simulated damage in the stiffened panel while suppressing the "louder" impacts.

Chengyang Huang; Ali Zare Hosseinzadeh; Francesco Lanza di Scalea, Experimental Mechanics & NDE Laboratory, University of California, San Diego, 9500 Gilman Drive, La Jolla, CA 92093, U.S.A.

INTRODUCTION

Composite materials are widely adopted in aerospace engineering for their superior strength-to-weight ratios, making them ideal for lightweight, high-performance structures [1]. Structural Health Monitoring (SHM) of plate-like composites often employs ultrasonic guided waves, which propagate over large areas and sensitively interact with damage. In a typical in-situ SHM setup, a sparse array of piezoelectric transducers both excites and receives guided-wave signals, and imaging is achieved by cross-correlating measured data to modeled wavefields ("replicas") at each location [2]. Conventional delay-and-sum (DAS) beamforming treats the replica as a simple time-shifted impulse, performing a zero-lag cross-correlation between the measured signal and a Dirac delta function [3]. While effective for bulk waves, this approach fails to account for guided-wave dispersion, multiple propagation modes, and boundary reflections inherent to complex composite structures [4]. To overcome these limitations, Reverse Time Migration (RTM) methods cross-correlate the forward-propagated experimental wavefield with a replica derived from the medium's true Green's functions [5]. By using the actual dispersive, multimode response of the structure, RTM achieves superior focusing and defect localization without requiring narrowband filtering or group-velocity tracking [6].

Beyond DAS and RTM, high resolution imaging has been pursued using advanced array processing techniques in the Match Field Processing (MFP) framework that exploit the signal and noise subspaces of the measurement covariance matrix [7]. Algorithms such as MUSIC (Multiple Signal Classification) identify scatterer locations by orthogonalizing array responses against noise subspaces [8]. However, MUSIC-type methods hinge critically on selecting a threshold to separate signal and noise subspaces, which could be significantly complicated by finite scatterer sizes, multimodal dispersion, and reflections from structural features such as stiffeners and boundaries [9]. The need to model near field effects, temperature variations, and material anisotropy further increases replica-model mismatch, undermining algorithmic robustness [10-11]. To address these challenges, the coherent White Noise Constraint (C-WNC) beamformer formulates imaging as a minimum-variance optimization problem with an explicit constraint on the white noise gain [12]. Instead of factorizing the covariance matrix, C-WNC inverts it adaptively from measurements to derive optimal replica vectors, thereby minimizing modeling errors and achieving both high resolution and contrast in active defect imaging [13].

In parallel, passive sensing strategies have been extensively studied to relieve the need for active transmitters in the measurement of Green's function. Lobkis and Weaver showed that, under diffuse excitation, the time-averaged cross-correlation between two sensor signals converges to the undistorted Green's function, effectively transforming one receiver into a virtual transmitter [14]. Extending this concept, segmental-averaged Normalized Cross-Power Spectrum (NCPS) techniques suppress undesired power spectra components as a form of deconvolution operation to build a passive transfer matrix. Averaging over causal and acausal components further relaxes the requirement for a fully diffused field and enhances sensitivity to defect scattering [15].

Building on these foundations, this paper presents a data-driven MFP imaging framework tailored to stiffened carbon-fiber composite panels representative of commercial aircraft. By using experimentally measured replicas, optimal virtual time reversal is achieved without explicit modeling of guided wave complexities. The

broadband C-WNC beamformer is employed for active imaging, delivering sharp focus and robust contrast without subspace decomposition. Finally, principles of passive NCPS reconstruction are incorporated to generate a virtual active transfer matrix from sparse, uncontrolled excitations, obviating baseline subtraction and specialized time-windowing. Experimental results confirm that this combined approach significantly improves damage detectability in challenging composite structures.

METHODOLOGY

This section breaks down the imaging process of a successful SHM scheme into three primary steps: (i) acquisition of Green's function, (ii) optimum modeling of replica wavefield, and (iii) robust beamforming with a transducer array.

I. PASSIVE RECONSTRUCTION OF GREEN'S FUNCTION

Consider a linear time-invariant medium, e.g. a stiffened composite panel. The objective is to measure the structural Green's function between two points in the medium. For monitoring transient impact, a passive modality is typically employed to measure the Green's function from the pixel of impact p to a transducer element n, as in Figure 1(a). The system output is the reception signal R_n as a function of uncontrolled excitation E, uncorrelated noise N_n, and transducer response T_n. For monitoring an existing damage, an active modality is typically employed to highlight the transfer function between a transmitter element m and a receiver element n, as in Figure 1(b). The ray path that includes wave scattering at the location of defect is usually of interest for comparison between the pristine and the damaged case. The passive reconstruction of the active ray path can relieve the need of high voltage D2A multiplexing for active sensing. As shown in Figure 1(c), the transfer function between the two transducer elements can be reconstructed from the cross-correlation of the two reception signals. Practically, the Normalized Cross-Power Spectrum (NCPS) recovers the inter-element response with accurate phase and minimum magnitude distortion

$$NCPS_{nm}(\omega) = \frac{\langle R_m^*(\omega) R_n(\omega) \rangle}{\langle R_m^*(\omega) R_m(\omega) \rangle} = \frac{|E(\omega)|^2 |EM(\omega)|^2 K_{nm}(\omega)}{|E(\omega)|^2 |EM(\omega)|^2 + |N_m(\omega)|^2} \quad (1)$$

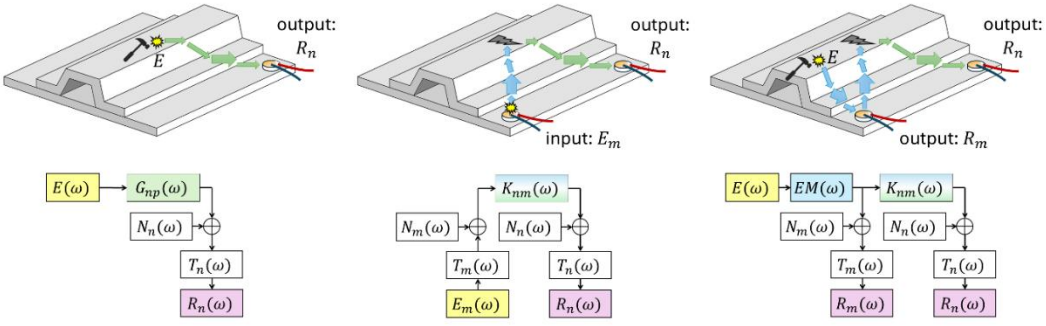

(a) Passive system (b) Active system (c) Passive reconstruction of active system

Figure 1. Ultrasonic imaging modalities for structural health monitoring applications. (a) Passive mode. (b) Active mode. (c) Passive reconstruction of an active transfer function.

where *EM* is the unknown Green's function from the excitation to the first receiver *m*. The ensemble averaged NCPS passive reconstructs the inter-element response function K_{nm} as if the first receiver m acts as a "virtual transmitter" that illuminates the active ray path as in Figure 1(b). It is worth noting that the presence of uncorrelated noise power spectrum in the denominator naturally stabilizes the deconvolution operation by avoiding extremely small values at the denominator of the NCPS.

II. DATA-DRIVEN MATCHED-FIELD PROCESSING

The time reversal (whether physical or virtual) can be written as a cross-power spectrum between the reception signal *R* and its time-reversed replica *w*, which exhibits the form of Bartlett beamformer in the MFP framework. It is easy to show that such a linear beamformer is a zero-lag cross-correlation in the time domain (similar to RTM)

$$I^{\mathrm{BAR,ideal}}(\overrightarrow{r_p}) = \int_{-\infty}^{\infty} w^*(\overrightarrow{r_p},\omega)R(\omega)\,d\omega = 2\pi\, Corr_{w,R}(\overrightarrow{r_p},\tau=0) \qquad (2)$$

where the best focus exist when the two signals are optimally matched (most similarity). As shown in Figure 2, three replica options are compared through their enveloped cross-correlation with the data. The data signal is a realistic experimental guided wave reception with dominant flexural mode and other weaker reflections. Using the data-driven approach, the same signal is replicated as the model. All waveguide complexities are inherently captured in the model, such as dispersion, mode conversion, and boundary reflections. The cross-correlation output shows significantly improved signal compression at the main lobe compared to other models.

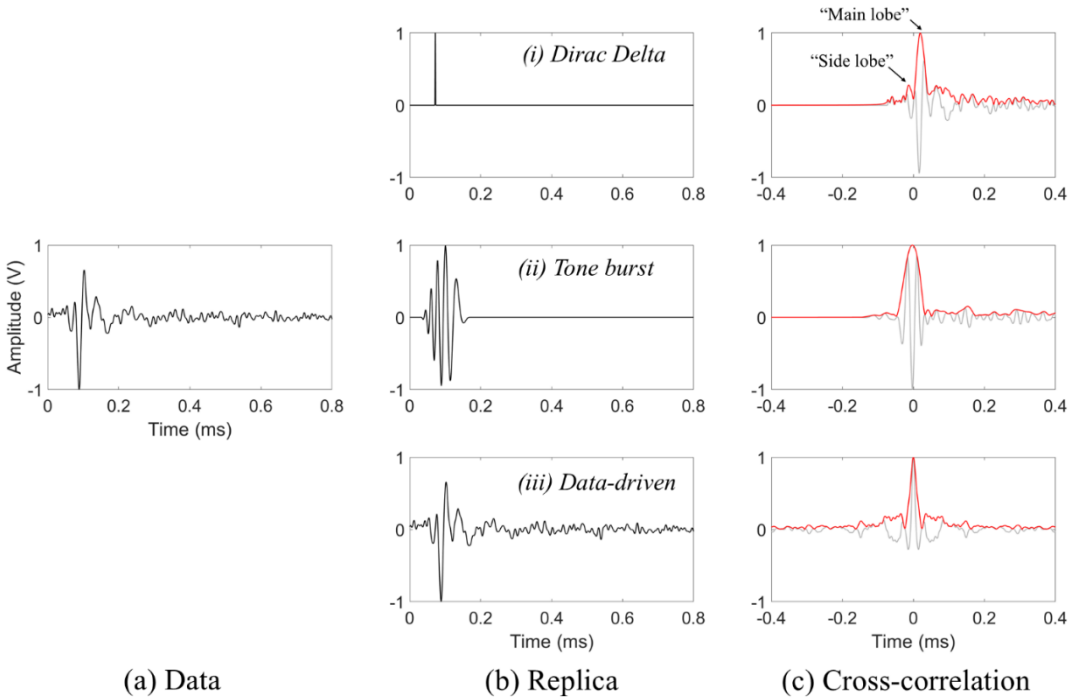

Figure 2. Benefits of using an informative replica signal in virtual time reversal. (a) The target guided wave signal to be backpropagated. (b) Choices of a replica signal using (i) Dirac Delta, (ii) tone burst, and (iii) the same experimental data. (c) Virtual time reversal interpreted as zero-lag cross-correlation.

III. COHERENT WHITE NOISE CONSTRAINT BEAMFORMING

For imaging complex composite structures with inherent low SNR, an incoherent average over the bandwidth may not result in a satisfactory zero-phase summation at the focus. It is preferable to exploit full signal complexity by adding cross-tone inner products to the covariance matrix based on the simple fact that noise is uncorrelated. One way is to stack the single-tone data vectors over frequencies in a "supervector". A coherent linear beamformer can thus be rewritten in the quadratic power output

$$I^{\mathrm{C-BAR}}\left(\overrightarrow{r_p},\Omega\right) = \widetilde{w}^{\mathrm{H}}(\overrightarrow{r_p},\Omega)\tilde{C}(\Omega)\widetilde{w}(\overrightarrow{r_p},\Omega) \tag{3}$$

where the covariance matrix is the expectation of the outer product of the passive data supervector. In the context of active sensing, the covariance matrix is the outer product of the active transfer matrix. It can be easily shown that the active transfer matrix can be decomposed into its column supervectors D_m as follows

$$\tilde{C}(\Omega) = \langle\widetilde{K}(\Omega)\widetilde{K}^{\mathrm{H}}(\Omega)\rangle = \frac{1}{N_{snap}}\sum_{N_{snap}}\sum_{m=1}^{M}\widetilde{D_m}(\Omega)\widetilde{D_m}^{\mathrm{H}}(\Omega) \tag{4}$$

where the subscript m denotes a (virtual) transmitter. Such decomposition shows that the covariance matrix describes the active system by averaging the responses from transmitters to scatterers while coherently enhancing the responses from the scatterers to receivers. As a result, in the MFP framework the passive Green's function G_{mp} should be considered as the data/replica.

For the supervector MFP formulation, the covariance matrix is rank deficient, which prevents the use of minimum-variance approach to optimize the replica vectors. The White Noise Constraint (WNC) algorithm solves rank-deficiency by imposing an inequality constraint on the gain against the spatial white noise. The minimum variance problem can be formulated by finding the minimum of function F as follows

$$F = \widetilde{w_{\mathrm{WNC}}}^{\mathrm{H}}\left(\overrightarrow{r_p},\Omega\right)(\tilde{C}(\Omega) + \varepsilon(\overrightarrow{r_p})I)\widetilde{w_{\mathrm{WNC}}}\left(\overrightarrow{r_p},\Omega\right) + \gamma(\widetilde{w_{\mathrm{WNC}}}^{\mathrm{H}}\left(\overrightarrow{r_p},\Omega\right)\widetilde{w}(\overrightarrow{r_p},\Omega) - 1) \tag{5}$$

where ε is the amount of spatial white noise added to invert the covariance matrix. The white noise ε is determined by setting the maximum norm of the optimized replica to be smaller than a fixed white noise constraint G_W at each pixel. The solution to the WNC optimization problem in the supervector form is

$$\widetilde{w_{\mathrm{WNC}}}\left(\overrightarrow{r_p},\Omega,G_{\mathrm{W}}\right) = \frac{(\tilde{C}(\Omega)+\varepsilon(\overrightarrow{r_p})I)^{-1}\widetilde{w}(\overrightarrow{r_p},\Omega)}{\widetilde{w}^{\mathrm{H}}\left(\overrightarrow{r_p},\Omega\right)(\tilde{C}(\Omega)+\varepsilon(\overrightarrow{r_p})I)^{-1}\widetilde{w}(\overrightarrow{r_p},\Omega)} \tag{6}$$

RESULTS

Figure 3 shows the test Carbon Fiber Reinforced Polymer (CFRP) panel used in this study. The panel consists of a skin and a co-cured hat-shape stringer, representing modern aircraft structure. Both components are made of 16-ply CFRP laminates in a quasi-isotropic layup. A 12-element array of piezoelectric transducers (PZTs) with a diameter of 8 mm was attached to the surface. Figure 3(b) shows the simulated damage case by sticking an added mass to the surface of the stringer flange with adhesive clay.

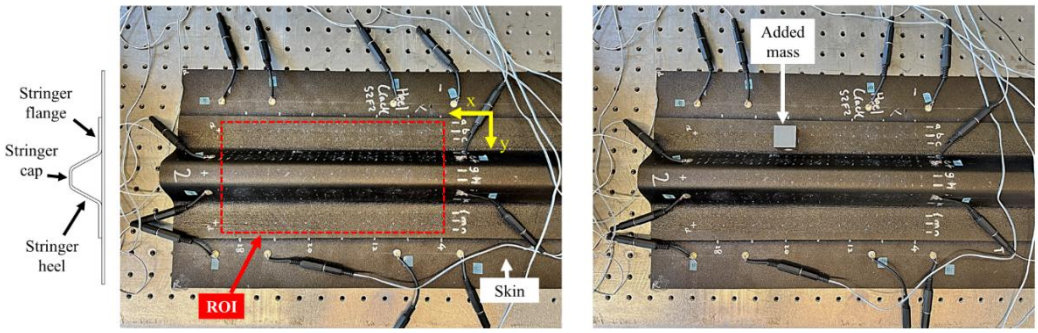

Figure 3. The test stiffened composite panel with a12-element sparse PZT array. (a) Pristine case with no added damage. The experimentally acquired Green's functions were sampled at a 1 cm spatial grid in the ROI. (b) Damaged case with an added mass attached to the stringer flange.

Figure 4 shows the imaging results of detecting simulated damage. Before the attachment of the added mass, the replica vectors were passively recorded by the array with controlled hammer excitations at each pixel in the ROI as boxed in Figure 3(a). The damage can be treated as a circular shape of the clay with a diameter of 2 cm. The bandwidth is set to 40-55 kHz. Figure 4(b) shows a comparison between actively measured K_{nm} (top) versus passively reconstructed transfer function. The active modality shows a phase lag due to transducer tuning. The passive reconstruction shows accurate phase, with more robust result obtained by averaging the NCPS over the causal and acausal counterpart. Figure 4(c) and (d) compare the beamforming results using coherent processors with raw NCPS versus averaged NCPS. Only two snapshots of uncontrolled hammer impacts are used for excitation of guided waves. The rank of the covariance matrix is augmented by the 12 virtual transmitters to 24. Using a 1 kHz sampling interval, the total degree of freedom is 12*16 = 192. The C-BAR beamformer shows large intensities on the right boundary of the simulated defect for both options. This is due to the biased illumination of the structure using excitations at only one location (the field is non-diffused). The C-WNC images show much better focus by rejecting most of the side lobes to below -100 dB. Such a large dynamic range is a result of power output bias of WNC beamformers due to rank-deficiency. For the raw NCPS result, the largest response is seen at one of the side lobes around the transducers. This is the near field "blind zones" due to the large zero-lag responses of passive reconstruction. For the causal-acausal averaged NCPS, these near field effects are largely suppressed, and the 0 dB response is seen at the lobes around the defect. It is also worth noting that there is a large response at the excitation location E, since the source is still correlated to the dominant eigenmodes in the covariance matrix.

The theory of passive reconstruction suggests that the full recovery of the Green's function requires the wavefield to be fully diffused, which is only available in the long recording noise (also known as coda waves). For most imaging applications with a requirement of fast framerate, the recording time is limited, which cannot relieve the spatially biased reception as seen in Figure 4. To improve the "unbalanced" passive reconstruction, a spatially distributed excitation is thus proposed as shown in Figure 5. By adding more excitation locations (thus rank contributions) to the covariance matrix, the passive system is "forced" to be unbiased from the excitations. The sensitivity to the source is also suppressed due to the averaging. It is shown that with more excitations, the C-WNC images can better show the lobe responses around the simulated damage.

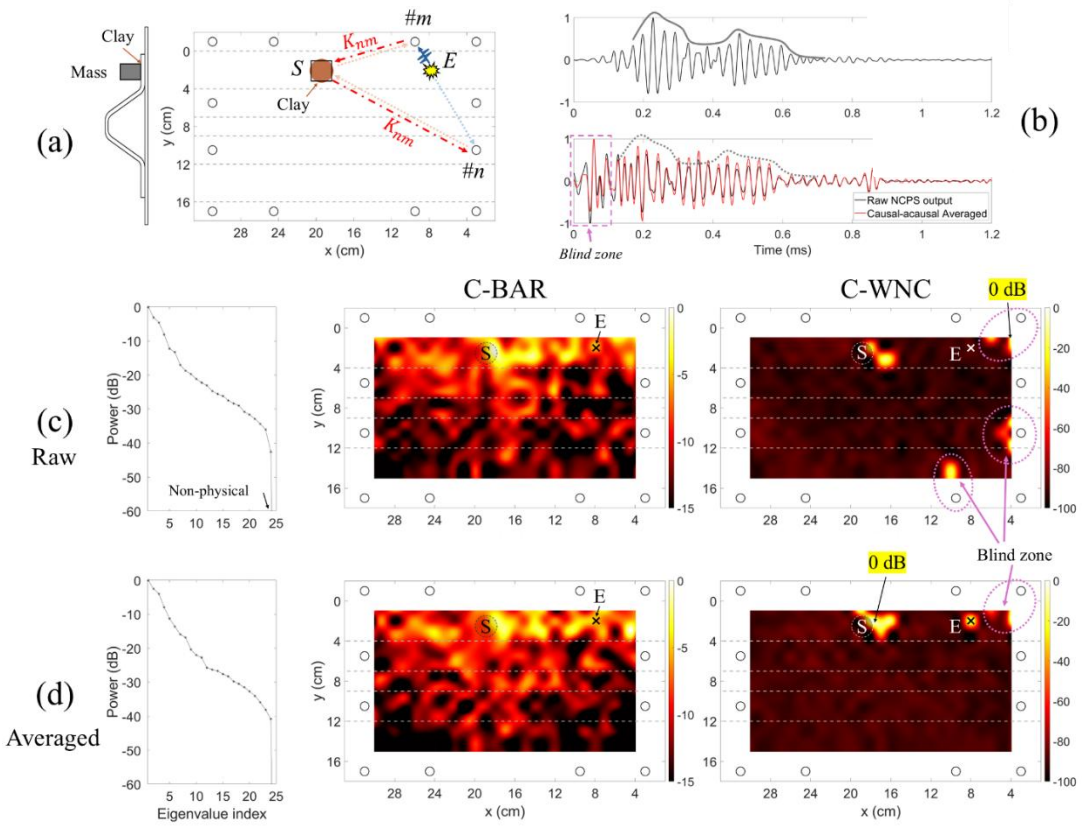

Figure 4. Defect imaging results using passively reconstructed transfer matrix with two snapshots of a hammer impact at one location. (a) Schematic showing the location of the simulated defect scatterer *S*, the impact location *E*, and two example receiver elements *#m* and *#n*. (b) Comparison of the ideal active transfer function from defect scattering (top) and passive reconstruction between the two elements (bottom). (c) Eigen structure of the covariance matrix composed of raw NCPS output, and imaging results using C-BAR and C-WNC. (d) Same as (c) but averaged with its causal and acausal counterparts.

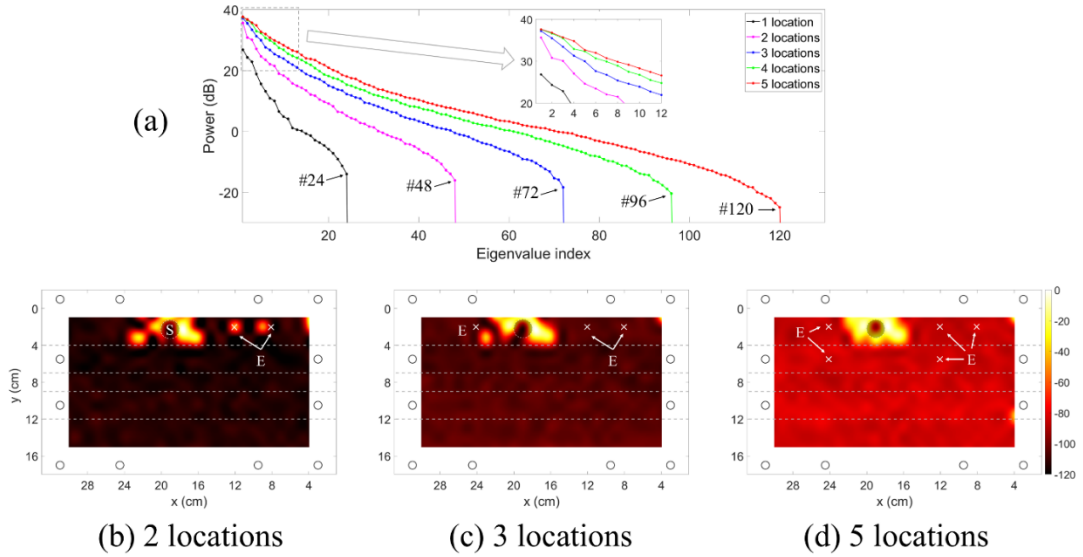

Figure 5. Defect imaging results using different hammer impact locations. Two snapshots are recorded at each marked location. (a) Variation of eigen structure of the covariance matrix when adding more excitation locations. Active mode C-WNC images using (b) 2, (c) 3, and (d) 5 locations of impacts.

CONCLUSION

This paper introduces a data-driven MFP framework for guided-wave ultrasonic imaging in complex structures, specifically targeting stiffened composite CFRP panels commonly found in aerospace applications. Rather than depending on intricate wave propagation models, the proposed approach constructs the replica wavefield directly from experimental measurements. Coherent MFP beamforming is achieved through frequency-domain cross-correlation of multi-tone replica and measured signals. Furthermore, the study incorporates passive reconstruction of active transfer functions using robust NCPS, reducing reliance on controlled source for SHM applications.

ACKNOWLEDGMENT

This research was funded by the U.S. Office of Naval Research (Agreement No. N00014-24-1-2481), by the U.S. Federal Aviation Administration Joint Center of Excellence for Advanced Materials (FAA Cooperative Agreement 12-C-AM-UCSD), and by MxV Rail through a University Grand Challenge Contract no. 24-0312-008622.

REFERENCES

1. Su, Z., L. Ye, and Y. Lu. 2006. "Guided Lamb Waves for Identification of Damage in Composite Structures: A Review," *J. Sound Vib.*, 295:753–780.
2. Wang, C. H., J. T. Rose, and F. K. Chang. 2004. "A Synthetic Time-Reversal Imaging Method for Structural Health Monitoring," *Smart Mater. Struct.*, 13:415.
3. Michaels, J. E. 2008. "Detection, Localization and Characterization of Damage in Plates with an In Situ Array of Spatially Distributed Ultrasonic Sensors," *Smart Mater. Struct.*, 17:035035.
4. Aslam, M., J. Park, and J. Lee. 2024. "A Comprehensive Study on Guided Wave Dispersion in Complex Structures," *Int. J. Mech. Sci.*, 269:109089.
5. He, J., and F. G. Yuan. 2015. "Damage Identification for Composite Structures Using a Cross-Correlation Reverse-Time Migration Technique," *Struct. Health Monit.*, 14:558–570.
6. Rao, J., A. Saini, J. Yang, M. Ratassepp, and Z. Fan. 2019. "Ultrasonic Imaging of Irregularly Shaped Notches Based on Elastic Reverse Time Migration," *NDT & E Int.*, 107:102135.
7. Baggeroer, A. B., W. A. Kuperman, and P. N. Mikhalevsky. 1993. "An Overview of Matched Field Methods in Ocean Acoustics," *IEEE J. Oceanic Eng.*, 18:401–424.
8. Schmidt, R. 1986. "Multiple Emitter Location and Signal Parameter Estimation," *IEEE Trans. Antennas Propag.*, 34:276–280.
9. Pierri, R., and F. Soldovieri. 1998. "On the Information Content of the Radiated Fields in the Near Zone over Bounded Domains," *Inverse Probl.*, 14:321.
10. Bao, Q., S. Yuan, and F. Guo. 2020. "A New Synthesis Aperture-MUSIC Algorithm for Damage Diagnosis on Complex Aircraft Structures," *Mech. Syst. Signal Process.*, 136:106491.
11. Yang, X., K. Wang, P. Zhou, L. Xu, J. Liu, P. Sun, and Z. Su. 2022. "Ameliorated-Multiple Signal Classification (Am-MUSIC) for Damage Imaging Using a Sparse Sensor Network," *Mech. Syst. Signal Process.*, 163:108154.
12. Cox, H., R. Zeskind, and M. Owen. 1987. "Robust Adaptive Beamforming," *IEEE Trans. Acoust. Speech Signal Process.*, 35:1365–1376.
13. Huang, C., and F. Lanza di Scalea. 2025. "High Resolution Ultrasonic Imaging of Extended Targets via Combined Match Field and Time Delay Beamforming," *Ultrasonics*, 145:107464.
14. Lobkis, O. I., and R. L. Weaver. 2001. "On the Emergence of the Green's Function in the Correlations of a Diffuse Field," *J. Acoust. Soc. Am.*, 110(6):3011–3017.
15. Huang, C., A. Z. Hosseinzadeh, and F. Lanza di Scalea. 2024. "Ultrasparse Ultrasonic Synthetic Aperture Focus Imaging by Passive Sensing," *IEEE Trans. Ultrason. Ferroelectr. Freq. Control*, 71(5):518–535.